

The formation mechanism and morphology of Nickel particles produced by an ultrasound-aided spark discharge in liquid mediums

Yifan Liu¹, Xianglong Li^{1*}, Yan Li¹, Wu Zhao¹, Fushi Bai²

¹College of Manufacturing Science and Engineering, Sichuan University, Chengdu, Sichuan 610065, China

²Institute of Dynamics and Vibration Research, University of Hannover, Hannover, 30167, Germany

*Corresponding author: lixianglong@scu.edu.cn

ABSTRACT

Spark discharge is widely applied to fabricate the small scale particles. The ultrasound-aided spark discharge process is based on an electrical discharge in liquid media in the electrical discharge machining (EDM). The morphology, element composition, and crystal structure of Nickel particles were observed analyzed by SEM, EDS and XRD, respectively. The EDS and XRD indicated a high purity nickel particle generated in pure water. Plus, the effects of dielectric mediums on the size distribution were investigated. The size distribution of particles in pure water is narrower than in kerosene. This distribution is remarkable after the ultrasound is introduced into the generating process. **Based on the attaching and entrapping processes, the formation mechanism of different structural particles was interpreted.** The results serve as a guide for the future research on controlling the particle properties such as size and morphology through improving the experimental conditions.

Keywords: ultrasound-aided spark discharge, dielectric mediums, particle purity, size distribution, formation mechanism

1. Introduction

The need for metallic micro/nanoparticles in science and technology is constantly increasing, in the fields ranging from semiconductor research and industry to environmental research. Metallic micro/nanoparticles with the size dependent properties have been found to be applied in numerous fields, such as Nano electronics, sensor technology, linear optics, catalysts, hydrogen storage and solar technology etc. [1-2]. Various kinds of metallic micro/nanoparticles have been produced by a variety of physical methods like gas-evaporation, vapor condensation, plasma, laser ablation, and spark discharge [3-6]. Spark discharge is receiving increased attention as a method for producing metallic micro/nanoparticles due to the simple and low cost of construction and operation of the setup. This technique employs periodic spark discharge to vaporize electrode materials and subsequently form micro/nanoparticles via the process of **nucleation and condensation**. During the spark discharge, the breakdown voltage causes a discharge channel formed instantaneously between the electrode gaps through the dielectric fluid. The subsequent plasma is formed to make the local temperature of the spark reach approximately 10000-18000 K [7]. Material is removed through the thermal erosive action of electrical discharges between the two electrodes. Every spark discharge melts and evaporates a small amount of material from both the electrodes. Most of the molten metals and vapor clusters are ejected to form particles when they come in contact with the cold dielectric mediums. Nguyen and Berkowitz [8] produced high purity magnetized particles by spark erosion. Hontanon [9] synthesized the copper micro/nanoparticles in pure nitrogen by the electrical discharges between two electrodes. In this research, the electrical gap and the gas flow rate mainly determined the yield and size distribution. Schmidt-Ott [10] investigated the characterizations of

1 Silicon nanoparticles produced by spark discharge and concluded the relationship between purity of
2 nanoparticles and the synthesizing conditions. Messing and Knut Deppert [11, 12] produced Pd
3 particles in an aerosol generator and characterized them with different photoelectric devices. They
4 confirmed that the small size dispersion and particle surface coverage could be controlled. Tabrizi [6,
5 13-14] used the microsecond spark discharge generator to synthesize bimetallic nanoparticles with
6 an arbitrary mixing on nanoscales. Voloshko and Itina [15, 16] had numerically investigated the
7 formation of metallic micro/nanoparticles via elucidating physical mechanisms and thermodynamic
8 analysis to compare the nucleation rate and particles size in two methods. Anis [17] synthesized Ni
9 and Pt nanomaterials in acidic and alkaline solutions via glow discharge to verify the two kinds of
10 synthesis mechanisms. Dvornik [18] used spark erosion to produce micro-structured particles and
11 carbonized them in CO gas to synthesize nanostructured particles. These researchers mainly used a
12 high voltage (over than 1KV) to generate energy and a flowing solution like gas or liquid to take
13 away the primary particles to form nanoparticles after nucleation and condensation. Hence, these
14 methods depended on sealed chamber, which allowed for turbulence in the gas or liquid flow. Plus,
15 the insulation of the chamber should be noticed due to the high voltage. Some researchers also used
16 electrical discharge machining (EDM) to fabricate particles with a low voltage(less than 200V). Sahu
17 [19] mainly used micro-EDM to prepare the copper micro/nanoparticles with different operating
18 parameters in deionized water added stabilizers. Tseng [20] used the EDM device to fabricate silver
19 nanoparticles in water at room temperature. However, these researches did not discuss the forming
20 mechanisms of solid or hollow particles. In our previous research [21, 22], we found that hollow
21 monometallic particles could be fabricated via the EDM device with the assist of the ultrasound.
22 Compared with the solid micro/nanoparticles, the hollow micro/nanoparticles have large-specific
23 surface area, high-specific surface energy, and catalytic activity, and have different properties from
24 conventional particles, such as optics, magnetics, mechanics, electricity, and chemical activity [23].
25 Therefore, the preparation of hollow metallic micro/nanoparticles has become hot research topic in
26 recent years. Peng [24] fabricated the hollow Ni microspheres via silicon powder-mixed spark
27 discharge. They mainly focused on the size distribution related to the varying operation conditions.
28 Byeon [25] used the spark plasma to synthesize bimetallic hollow micro/nanoparticles in ambient gas
29 as storing material like Lithium storage capacity. The purity of powders was affected obviously by
30 the added element in the generation surrounding. In terms of the hollow monometallic particles,
31 Nersessian and Berkowitz [26, 27] focused on producing hollow monometallic particles in nitrogen
32 surrounding with this method. Unfortunately, they didn't pay more attention to the formation
33 mechanism of hollow particle, and the mean size of their productions was large. The purity also was
34 affected by the Nitrogen. Hence, in terms of the formation mechanism and morphology of different
35 structural particles, especially for the hollow metallic particles, the research is not enough.

36
37
38
39
40
41
42
43
44
45
46
47
48 In this paper, we mainly focused on investigating the formation mechanism and morphology of
49 hollow Ni micro/nanoparticles generated by ultrasound-aided Spark Discharge. To investigate the
50 purity of particles generated in different dielectric mediums (pure water and kerosene), the element
51 composition and lattice structure of samples were detected by EDS and XRD, respectively. To
52 discuss the positive effect of ultrasound on the size of particles, the relationship between cavitation
53 collapses and the dielectric mediums properties was studied through analyzing the influence of
54 surface tension, viscosity, and vapor pressure on the cavitation. The higher purity and narrower size
55 distribution were obtained in pure water. Finally, based on the attaching and entrapping processes,
56 the formation mechanism of different structural particles was interpreted. Especially, the formation
57
58
59
60
61
62
63
64
65

mechanism of hollow particles were illustrated in detailed.

2. Experimental details

Fig.1 shows the schematic diagram of our ultrasound-aided EDM experimental setup developed to produce Ni particles. The system consists of a spark discharge generator and an ultrasound generator. The spark energy is obtained by a numerical control EDM machine E46PM (Jiangsu Excellent Numerical Control Equipment Co., Ltd., Jiangsu, China) with a variable electrical current ranging from 1.5 to 60 A, a variable pulse width ranging from 2 to 1200 μ s, and a variable gap voltage ranging from 30 to 120 V. The servo system controls the tool electrode to maintain an optimal distance in micrometers. The ultrasound oscillators are attached on opposite sides of the stainless steel processing box. We conducted the high purity Ni rods (purity better than 99.9%, Tianjin Chengshuo Steel Trading Co., Ltd., Tianjin, China) as two-electrode; the tool electrode (cathode) and workpiece electrode (anode).

The present investigation was conducted in a laboratory environment with the pure water and kerosene. The boiling point of kerosene ranges from 180 to 310 $^{\circ}$ C and density is 0.780g/cm³ at 25 $^{\circ}$ C. For the pure water, the density is 1g/cm³ at 25 $^{\circ}$ C. The physical characters of the two dielectric medium are shown in the table1.

Table1. The physical characters of pure water and kerosene [29]

Dielectric Medium	Viscosity	Surface tension	Vapor pressure
	10 ⁻⁶ (m ² /s)	10 ⁻² (N/m)	mmHg
Pure water	0.659	7.28	23.8
Kerosene	2.5-2.7	2.3-3.2	45-56

In our research, groups of experimental parameters with an orthogonality relation had been applied. The current ranged from 4.5 to 60 A, pulse width ranging from 15 to 300 μ s, and a variable gap voltage ranged from 15 to 90 V. The ultrasound power ranged from 0-900W and frequency selected the 28, 56, and 126 KHz. For the findings of this paper, the results had a similar tendency and changing rule. Here, two groups of samples were selected to represent the findings. The experimental group was applied by a 15A current, 300 μ s pulse width, 45V gap voltage, 900 W power, and 28 KHz frequency with a fixed time (1 hour). The control group was applied by the same experimental parameters without the ultrasound as well as one hour. The samples were washed and cleaned with petroleum ether (melting (II), AR, boiling point 60–90 $^{\circ}$ C, 500 mL, Hangjia Bio-pharmaceutical Technology Co., Ltd. Chengdu, China). The particles were observed by scanning electron microscope (SEM; Hitachi S-4700; Hitachi Ltd., Tokyo, Japan) to analyze particle surface morphologies. The composition analysis was carried out by energy-dispersive energy dispersive spectroscopy (EDS; JSM-7500F, JEOL, Japan). The crystal structure was identified by X-ray diffraction (XRD; X'Pert Pro MPD, Philips, Netherlands). The scanning range was from 15 $^{\circ}$ to 90 $^{\circ}$ using Cu K α ($\lambda = 1.54056\text{\AA}$) and operated at 40 kV and 200mA. The step size of 0.02 $^{\circ}$ and scan rate of 5 $^{\circ}$ per min were used for recording the XRD spectra of samples. The X-ray spectrum was analyzed based on the standards presented by the Joint Committee on Powder Diffraction Standards (JCPDS, data file PDF #65-0380). Structure refinement was performed using MDI JADE 5.0 software, which can perform powder diffraction data analysis and acquisition.

3. Results and Discussion

3.1 The EDS and XRD analysis of particles produced in two dielectric mediums

The EDS and XRD spectrum were performed to detect respectively the material composition of the particles and purification of crystallization process in different dielectric mediums. The analysis

1 results of particles generated with the kerosene and pure water are shown in the Fig.2 and Fig.3,
2 respectively. The EDS results show that the samples mainly contained three elements including
3 Carbon(C), Oxygen (O), and Nickel (Ni). The results are shown in table2.

4 Table 2. The EDS analysis datasheet of Ni particles in different dielectric mediums.

5

Elements	Mass (%)	
	Pure water	Kerosene
C	0.38	3.83
O	1.78	1.76
Ni	97.84	94.41
Totals	100	100

6
7
8
9
10
11
12
13

14 For the kerosene, the proportions of three elements are 3.83%, 1.76%, and 94.41%, respectively.
15 For the pure water, the proportions are 0.38%, 1.78%, and 97.84%, respectively.

16 The XRD spectrums show that the spark generated Ni particles in different dielectric mediums
17 were face-centered cubic (FCC) crystallites. The peak patterns and peak positions for all diffraction
18 patterns closely match those for perfect FCC Ni (JCPDS, data file PDF #65-0380). We had not
19 observed any detectable impurity peaks related to Oxygen and Ni's oxides from the XRD patterns.
20 From the EDS results, 1.78% and 1.76% oxygen were detected respectively in the samples generated
21 in pure water and kerosene, and the proportions were almost invariable. To explain this discrepancy,
22 we regarded as the source of oxygen could come from the NiOx which did not been detected in XRD
23 due to the few proportions. It can be known that the Ni particles is hardly oxidized in Spark
24 Discharge. As for the resource of oxygen in kerosene, we confirmed that some oxygen dissolved in
25 the dielectric media.

26 From the table 2, the proportion of carbon of samples generated in the kerosene is ten times
27 than in the pure water. As the hydrocarbon, the kerosene consists of complex mixtures of aliphatic,
28 aromatic and polycyclic aromatic hydrocarbons. Hence, the presence of C in the sample is due to the
29 decomposition of kerosene in a high temperature. The decomposition of kerosene has an
30 endothermic reaction to break the C-H bond to generate carbon and hydrogen. The reduction of peak
31 intensity and the appearance of the diffuse peak around the diffraction peak illustrated that the
32 particles were formed with a particular impurity in the kerosene. The carbon atoms doped and
33 dissolved into octahedral interstitial sites as a result of forming the interstitial solid solution [28].
34 This doping behavior causes the decreasing of the purification of the particles generated in the
35 kerosene. The pure water does not contain a C element. Hence, the resource of 0.38% C from sample
36 generated in water is produced by the conductive tape which is used to as the fixer to analyze the
37 sample, and the measurement error is inevitable.

38 The proportion of Ni in pure water is near 98%, and the particles produced in the water had a
39 higher purity than the kerosene. The XRD pattern of sample generated in water did not show any
40 other additional peaks, indicating that a simple monometallic particle had been formed.

41 3.2 Effect of dielectric mediums on the size distribution

42 3.2.1 Effect of dielectric mediums on size distribution of particles generated by Spark Discharge 43 process

44 Fig.4 shows the effect of the dielectric type on the morphology and size distribution of the
45 submicron and micro particles.

46 It can be noticed that the mean particle sizes in pure water is smaller than the mean particle
47 sizes in kerosene for the same test conditions. The size distribution of particles in pure water is

1 narrower than in kerosene. As the Table1 shows, the viscosity of kerosene is higher than pure water.
2 The solidification time in sticky dielectric medium is longer than pure water. The hysteresis leads to
3 a behavior for the bigger particles.

4 **3.2.2 Effect of dielectric mediums on size distribution of particles generated by Ultrasound-Aided** 5 **Spark Discharge process**

7 Fig.5 shows the effect of the ultrasound waves on the morphology and size distribution of the
8 submicron and micron particles in different dielectric mediums. It can be found that the size
9 distribution has a remarkable change after aiding ultrasound. It is worth mentioning that the amount
10 of particles smaller than 5 μm particles is higher (more than 80%) than the productions generated
11 without ultrasound.
12

13 As for the influence of ultrasound waves on the size distribution, the ultrasound waves prevent
14 aggregation by a shearing action which can crack the weak bonds between large aggregated Ni
15 clusters. Hence, the particle size is decreased, which favors the formation of submicron and micro
16 particles with a small size. Plus, the size distribution also depended on the influence of dielectric
17 mediums properties on the occurrence and the intensity of cavitation. The effect of ultrasound
18 cavitation generates microbubbles and effectively prevents from aggregation of crystal grains in the
19 process of homogeneous nucleation. The dielectric mediums properties that affect the behavior of
20 ultrasound cavitation include viscosity, surface tension, and vapor pressure [30].
21

22 The viscosity of kerosene is higher than pure water, which results in that the attenuation of
23 sound intensity in a high viscosity liquid. It is not easy to occur a cavitation with a reduction of
24 sound intensity. The number of cavitating bubbles per unit volume is reduced. Hence, the viscosity
25 has a retarding effect on the cavitation. Because greater power input is required to break the
26 cavitation threshold [31]. For the low viscosity like pure water, acoustic cavitation occurs more
27 easily, because the ultrasonic intensity applied could more easily exceed the molecular forces of the
28 liquid. The vapor pressure of kerosene is high than pure water. More bubbles are created in the high
29 vapor pressure, but they collapse with less intensity due to a smaller internal/external pressure
30 differential [32]. The intensity of cavitation collapses in a low vapor pressure is more violent than
31 high one. Surface tension of dielectric mediums also influences cavitation behavior. Liquid having
32 high surface tension requires higher energy to produce cavitation bubbles, thus cavitation occurs
33 differently. However, when the cavitation occurs, the shrinkage force of bubbles with a high surface
34 tension becomes strong. The surface tension of pure water is three times than kerosene, which results
35 in a violent collapsing in the pure water. Collapse of the bubbles produces an extreme temperature
36 and pressure gradient between boundary layers and ambient areas of the bubbles. The large
37 temperature and pressure gradients resulting from collapsing of these bubbles lead to the dispersion
38 of the nanoparticles in the liquid media [33].
39

40 Hence, due to the effect of ultrasound on the dielectric mediums, the size distribution of
41 particles in water is narrower than in kerosene.
42

43 **3.3 Forming mechanism of nickel micro/nanoparticles by ultrasound -aided spark discharge**

44 **3.3.1 The formation mechanism of different structural Ni particles**

45 When the molten vapors occurred around the electrodes under superheated boiling conditions,
46 the primary particles were formed firstly by homogeneous nucleation of the supersaturated vapor or
47 liquids and subsequently transported into the dielectric fluid by a force caused between the
48 electrodes of about 280M Pa [34]. There are two original particles which generally form a bimodal
49 distribution—primary particles from condensed vapors tend to small particles, typically with a mean
50
51
52
53
54
55
56
57
58
59
60
61
62
63
64
65

1 diameter with a few nm (about 10nm), whereas the molten droplets are usually larger than 100nm.
2 All the two original particles are with homogeneous atomic clusters. Further growth of primary
3 particles by condensation and coagulation resulted in the productions with a micro or Nano size.

4 Atomic clusters start Brownian motion after they enter into the working solution, due to the
5 impact of the thermal motion of liquid molecules, and a part of them are easily to aggregate into
6 crystal grains. The formation process of the particles is the growth of the crystal grains particles. The
7 nucleation of the evaporated atoms and molten liquids from the electrodes in the decaying plasma
8 channel condenses to particles with a small size. The condensation process and the morphology can
9 be affected by the ambient environments, where any atom, particle, gas or bubbles leads to form
10 different structural particles.
11

12 Actually, in the spark situ, heating of spark plasma will produce mixed species from the Nickel
13 and dielectric medium, namely, Ni atoms and clusters, Ni aggregations and droplets, atomic and
14 molecular gas like hydrogen and oxygen in water or hydrogen and hydrocarbon in kerosene. **The
15 atomic and molecular gases, which are very active, will adsorb together to form bubbles between the
16 electrodes.** The cavitation effect also created fine bubbles in the liquid [35]. These bubbles affect the
17 aggregation process of Ni atoms and clusters, which results in forming different characteristic
18 structures.
19

20 The spark-produced metallic clusters in the spark gap attach on the gas/liquid interface, and
21 further aggregate to shells around the gas bubbles. It is known that the attachment of particles to gas
22 bubbles is a complex process, which is affected by many factors, such as particle surface properties,
23 particle size, bubble surface properties, electrostatic interactions, and hydrodynamic conditions.
24

25 We defined this attachment as “quasi-soft template”. In this generating process, the fine bubble
26 serves as a soft template. The templates directly determine the shape and approximate cavity size of
27 the resultant hollow structures. The shell thickness depends on the effect of absorption among atomic
28 clusters, crystal grains, small particles, and bubbles.
29

30 The schematic illustration of procedures for generating metallic particles by ultrasound-aided
31 spark discharge technique can be seen in Fig. 6.
32

33 During solidification, superheated metallic clusters are cooled instantaneously because of the
34 tremendous temperature gradient between surrounding dielectric medium and metallic corrosions
35 [37]. Subsequently, these corrosions are ejected by adiabatic expansion from the plasma channel in
36 the very beginning (as the route ①). When the metallic clusters interact with the gas environment,
37 there are two forming cases named entrapping and attaching.
38

39 In the case of entrapping, these bubbles (spark-induced bubbles and ultrasound-induced
40 microbubbles) are passively trapped into the interstition among the metallic clusters and nearly
41 insoluble in them. If the temperature is lowered rapidly, the metallic clusters will eventually undergo
42 a eutectic transition to a heterogeneous system including solid and gas. If the solubility limit is
43 reached, gas will precipitate out of the melt. Hence, the porosity forms during solidification (as the
44 route ②).
45

46 In the attaching case, the absorption and combination between gas bubbles and metallic
47 clusters play a significant role in the formation of the hollow particles. The clusters accumulate and
48 attach on the bubble interfaces while they encounter the bubbles. These bubbles have a dynamic
49 growing process. At the initial stage, the metallic nuclei combine with gas bubbles due to the
50 electrostatic adherence. Then, small size gas bubbles actively coagulate in the dispersion system to
51 form bigger bubbles which provide the spherical template. In the “quasi-soft template” cases, the
52
53
54
55
56
57
58
59
60
61
62
63
64
65

1 forming of hollow particles mainly depends on the absorption effect [38]. The heterogeneous
2 nucleation leads to the formation of substantial small crystal nuclei which are absorbed on the
3 surface of the bigger bubbles. The crystal nuclei rapidly cool and solidify to form a hollow particle
4 (as the route③). Plus, the growing process for each crystal grains cannot keep in the same step. The
5 shrinking of interface and the non-uniform distribution of mass cause a small shrinkage hole in the
6 particles (as the route④). When the metallic clusters attach on the partial surface of bubbles, some
7 flaked particles (as the route②) are cooled rapidly.
8

9 The absorption and attachment of the clusters on the bubble surface are restrict with the
10 interface motion. The clusters should have enough time to diffuse to the bubble interface which, in
11 turn, requires a long lifetime of the bubble. This requirement will be the breakthrough point in our
12 further research.
13

14 **3.3.2 The morphology of different structural Ni particles**

15 The morphologies of collected particles were observed under SEM. Most of them were shown
16 to be spherical particles with a solid structure. The others character different structures including
17 flaked particles, porous particles and hollow particles. The morphologies of different structures are
18 showed in Fig.7.
19

20 As illustrated in Fig7-A, most of particles are complete solid. This formation mechanism is in
21 accordance with the route①. According to the route⑤, some particles with a crack or a rupture-like
22 appearance are produced by the spark discharge as shown in the Fig.7-B. The Fig.7-C and D shown
23 that some flaked particles are generated as result of route②. We can find some hollow particles with
24 a thin shell from the Fig.7-I to Fig.7-K which are following the route③. Regarding to the route④,
25 some particles are formed with a small shrinkage hole (Fig.7-E to Fig.7-H). It is worth noting that
26 most of particles were ejected out the gap by the impulse heat explosion force which is formed
27 through an instantaneous high temperature of the discharge channel. In the whole system,
28 particle-particle collision leads to a sticking on the internal and external surface of particles, which
29 shows satellite shaped particles like Fig.7-H and Fig.7-L.
30

31 **Conclusions**

32 The electrical discharge machining aided by ultrasound method in a liquid environment is a
33 simple, effective technique to generate hollow particles with a small size. Our study described the
34 formation mechanism of different structural particles including solid particles, flaked particles,
35 porous particles and hollow particles based on the attaching and entrapping processes. EDS indicated
36 a high purity (98%) of nickel particles generated in pure water. The particles is hardly oxidized by
37 the oxygen decomposed by the high temperature from the XRD results.
38

39 The experimental results show that the viscosity, vapor pressure, and the surface tension of
40 dialectical mediums play an important role in determining the size distribution of submicron and
41 micron particles. Compared with the kerosene, the mean particle sizes in pure water is smaller than
42 the mean particle size in kerosene for all test conditions. The size distribution of particles in pure
43 water is narrower than in kerosene. This distribution is remarkable after the ultrasound has aided the
44 generation process. Hence, the work described here suggests that spark discharge aided by
45 ultrasound with pure water could be an optimal processing which generates high purity and small
46 metallic particles.
47

48 **Acknowledgements**

49 This work has been supported by the National Natural Science Foundation, China (Grant
50 No.51275324) and Innovation Method Fund of China (2013IM030500).
51
52
53
54
55
56
57
58
59
60
61
62
63
64
65

References

- [1] V.A. Vons, H. Leegwater, et al., Hydrogen storage properties of spark generated palladium nanoparticles, *Int. J. Hydrogen Energy*, 35(2010) 5479-5489.
- [2] J.P. Borra, Nucleation and aerosol processing in atmospheric pressure electrical discharges: powders production, coatings and filtration, *J. Phys. D: Appl. Phys.*, 39(2006) 19 - 54.
- [3] V. Abdelsayed, K. M. Saoud and M. Samy El-Shall, Vapor Phase Synthesis and Characterization of Bimetallic Alloy and Supported Nanoparticle Catalysts, *J. Nanopart. Res.*, 8(2006) 519-531
- [4] T. Ohno, Morphology of Composite Nanoparticles of Immiscible Binary Systems Prepared by Gas-Evaporation Technique and Subsequent Vapor Condensation, *J. Nanopart. Res.*, 4(2002) 255-260
- [5] V.S. Burakov, M.I. Nedelko, et al., Laser and Plasma Assisted Fabrication of Nanoparticles in Liquids, *Proceedings of the International Conference Nanomaterials: Applications and Properties*, 3(2014) 2-7.
- [6] N.S. Tabrizi, M. Ullmann, V.A. Vons, U. Lafont, A Schmidt-Ott, Generation of nanoparticles by spark discharge, *J. Nanopart. Res.*, 11(2009) 315-332.
- [7] K. Vokurka, J. Plocek, Experimental study of the thermal behavior of spark generated bubbles in water, *Exp. Therm Fluid Sci.*, 51 (2013) 84–93.
- [8] P.H. Nguyen, S.H. Jin, A.E. Berkowitz, MnBi particles with high energy density made by spark erosion, *J. Appl. Phys.*, 115(2014) 17A756.
- [9] E. Hontañón, J.M. Palomares, et al., The transition from spark to arc discharge and its implications with respect to nanoparticle production, *J. Nanopart. Res.*, 15(2013) 1957
- [10] V.A. Vons, L.C. de Smet, et al, Silicon nanoparticles produced by spark discharge, *J. Nanopart. Res.*, 13(2011) 4867-4879.
- [11] M.E. Messing, R. Westerstrom, B.O. Mueller, et al., Generation of Pd Model Catalyst Nanoparticles by Spark Discharge, *J. Phys. Chem, C*, 114(2010) 9257-9263.
- [12] M.E. Messing, K.A. Dick, L.R. Wallenberg, et al., Generation of size-selected gold nanoparticles by spark discharge for growth of epitaxial nanowires, *Gold Bull.*, 42(2009) 20 - 26.
- [13] N.S. Tabrizi, Q. Xu, et al., Generation of mixed metallic nanoparticles from immiscible metals by spark discharge, *J. Nanopart. Res.*, 12(2010) 247-259.
- [14] N.S. Tabrizi, Q. Xu, et al., Synthesis of mixed metallic nanoparticles by spark discharge. *J. Nanopart. Res.*, 11(2009) 1209-1218.
- [15] T.E. Itina, A. Voloshko, Nanoparticle formation by laser ablation in air and by spark discharges at atmospheric pressure', *Appl. Phys. B*, 2013, 113(3) 473-478.
- [16] A. Voloshko, J. Colombier, T.E. Itina, Comparison of laser ablation with spark discharge techniques used for nanoparticle production, *Appl. Surf. Sci.*, 336(2015) 143-149
- [17] A. Allagui, E.A. Baranova, R. Wüthrich, Synthesis of Ni and Pt nanomaterials by cathodic contact glow discharge electrolysis in acidic and alkaline media, *Electrochem. Acta*, 93(2013) 137-142.
- [18] M.I. Dvornik, Nanostructured WC–Co particles produced by carbonization of spark eroded powder: Synthesis and characterization, *Int. J. Refract. Met. Hard Mater.*, 28(2010) 523-528.
- [19] R.K. Sahu, S.S. Hiremath, P.V. Mamivannan, et al., Generation and Characterization of Copper Nanoparticles Using Micro-Electrical Discharge Machining, *Mater. Manuf. Processes*, 29(2014) 477 - 486.
- [20] K. Tseng, C. Liao, D. Tien, Silver carbonate and stability in colloidal silver: A by-product of the electric spark discharge method, *J. Alloys Compd.*, 493(2010) 438-440.
- [21] Y.F. Liu, X.L. Li, Y.T. Wang, et al., Effect of system parameters on the size distributions of hollow nickel microspheres produced by an ultrasound-aided electrical discharge machining process, *Particuology*, 17(2014)36-42

- 1 [22] Y.T. Wang, X.L. Li, Y.F. Liu, et al., Effect of Non-electrical Parameters on the Size of Nickel Microspheres
2 Produced by an Ultrasound-aided Electrical Discharge Machining, *Chin. J. Mech. Eng.*, 51 (2015) 195-200.
- 3 [23] L. David, Sr. Wilcox, B. Morris, Microsphere Fabrication and Applications: an Overview. *Materials Research*
4 *Society Fall Meeting*, 372(1994) 3-14
- 5 [24] H. Peng, D. Yu, X. Zhang, S. Wang, Y. Wen, Fabrication of hollow nickel micro-spheres with high degree of
6 hollowness by silicon powder-mixed spark erosion, *Int. J. Mach. Tool. Manu.*, 85(2014)131–134.
- 7 [25] J.H. Byeon, Y.W. Kim, Ambient Plasma Synthesis of Si-Fe Hollow Nanoparticles and Their Biocompatibility
8 and Lithium Storage Capacity, *Adv. Mater. Interfaces*, 1(2014) 1300134
- 9 [26] N. Nersessian, S.W. Or, G.P. Carman, et al., Hollow and solid spherical magnetostrictive particulate
10 composites, *J. Appl. Phys.*, 96 (2004) 3362-3365.
- 11 [27] A. E Berkowitz, H. Harper, D.J. Smith, Hollow metallic microspheres produced by spark erosion, *Appl.*
12 *Phys. Lett.*, 85 (2004) 940-942
- 13 [28] Y.F. Liu, X.L. Li, Y. Li, et al. , The lattice distortion of nickel particles generated by spark discharge in
14 hydrocarbon dielectric mediums, *Appl. Phys. A* (2016) 122:174
- 15 [29] W.M. Haynes. *Handbook of Chemistry and Physics*, 96th ed., CRC Press, Boca Raton, 2015.
- 16 [30] S. Majumdar, P. S. Kumar, A.B. Pandit., Effect of liquid-phase properties on ultrasound intensity and
17 cavitation activity. *Ultrason. Sonochem.*, 5 (1998) 113–118.
- 18 [31] J. Raso, P. Manas, R. Pagan, F. J. Sala. Influence of different factors on the output power transferred into
19 medium by ultrasound. *Ultrason. Sonochem.*, 5 (1999) 157–162.
- 20 [32] C. E. Brennen. *Cavitation and Bubble Dynamics*. Cambridge University Press. 2013.
- 21 [33] H. H. G. Jellinek., Degradation of Long Chain Molecules by Ultrasonic Tension on Cavitation Waves. VII.
22 Effect of Viscosity and Surface. *J. Polym. Sci.* 22 (1956) 149-152.
- 23 [34] H. Tsuchiya, T. Inoue, Y. Mori, *Proceedings of the Seventh International Conference on Electro machining*,
24 J.R. Crookall, North-Holland, Amsterdam, 1983.
- 25 [35] M. Hodnett, M. J. Choi, B. Zeqiri. Towards a reference ultrasonic cavitation vessel. Part 1: Preliminary
26 investigation of the acoustic field distribution in a 25 kHz cylindrical cell, *Ultrason. Sonochem.*, 14 (2007) 29–40.
- 27 [36] T.V. Pfeiffer, J. Feng, A. Schmidt-Ott, New developments in spark production of nanoparticles, *Adv. Powder*
28 *Technol.*, 25(2014) 56-70.
- 29 [37] Z. Yan, R. Bao, C.M. Busta, D.B. Chrisey, Fabrication and formation mechanism of hollow MgO particles by
30 pulsed excimer laser ablation of Mg in liquid, *Nanotechnology*, 22(2011) 1-8.
- 31
32
33
34
35
36
37
38
39
40
41
42
43
44
45
46
47
48
49
50
51
52
53
54
55
56
57
58
59
60
61
62
63
64
65

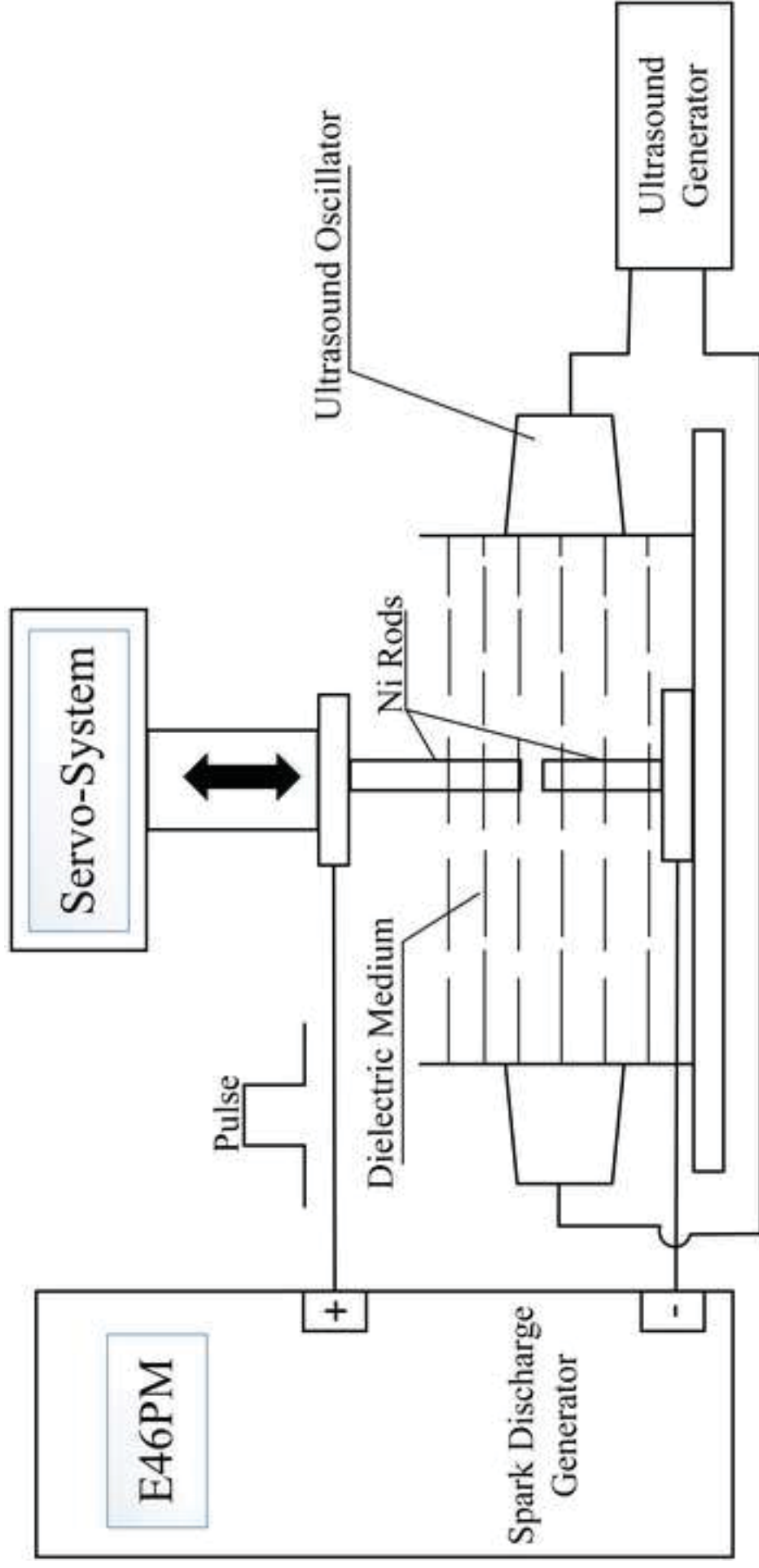


Figure 2
Click here to download high resolution image

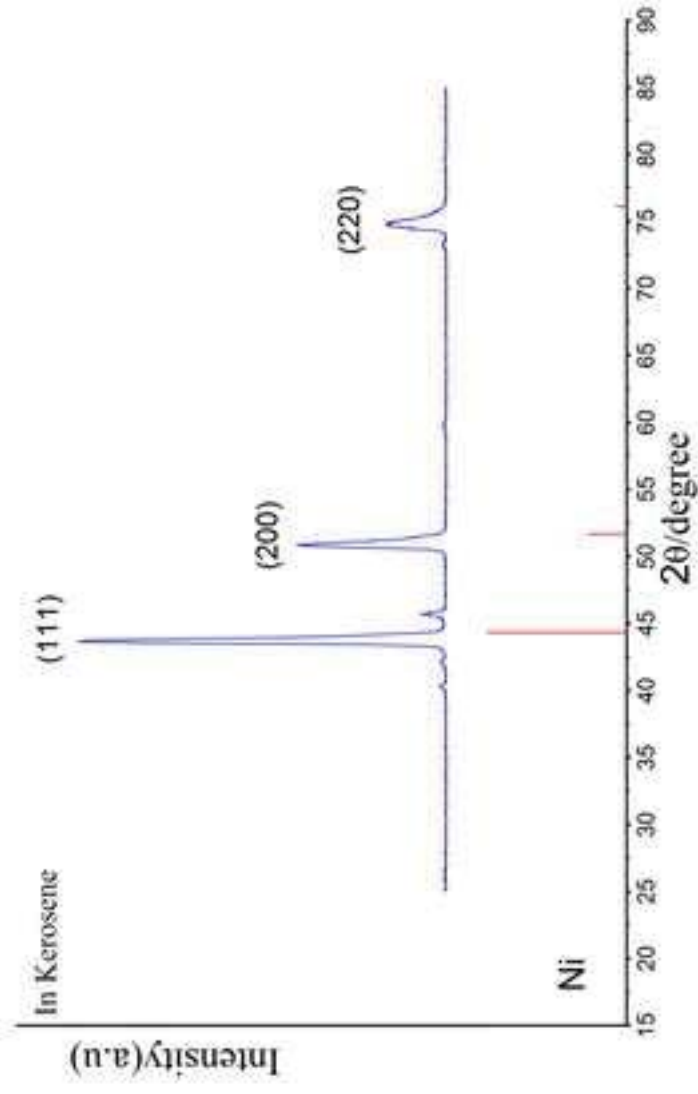
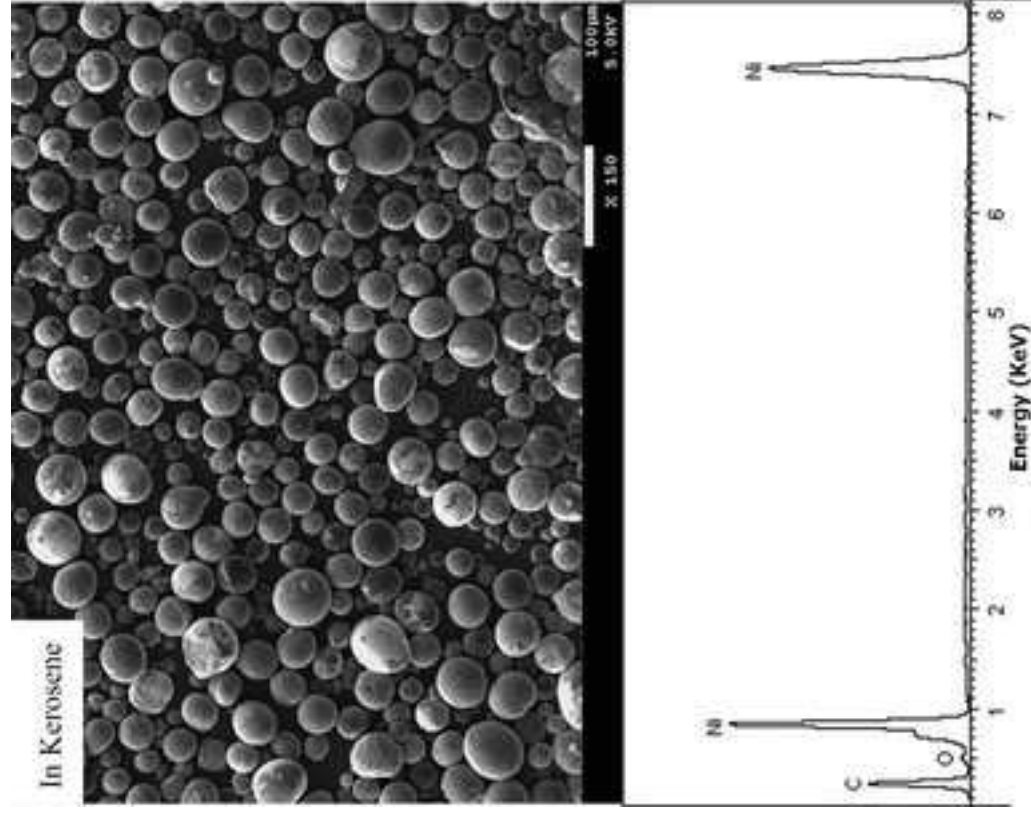


Figure 3
Click here to download high resolution image

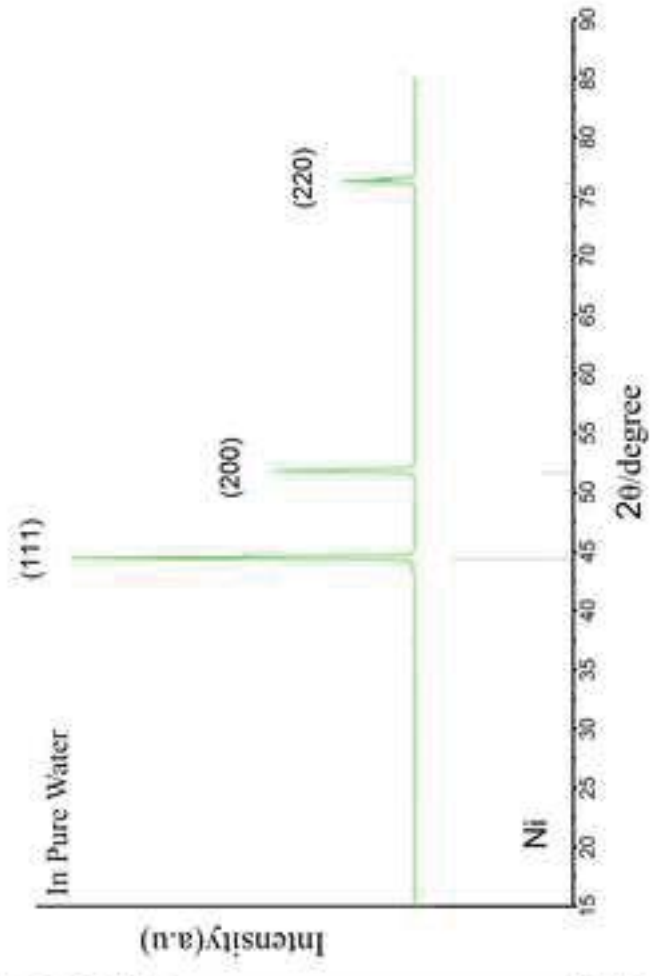
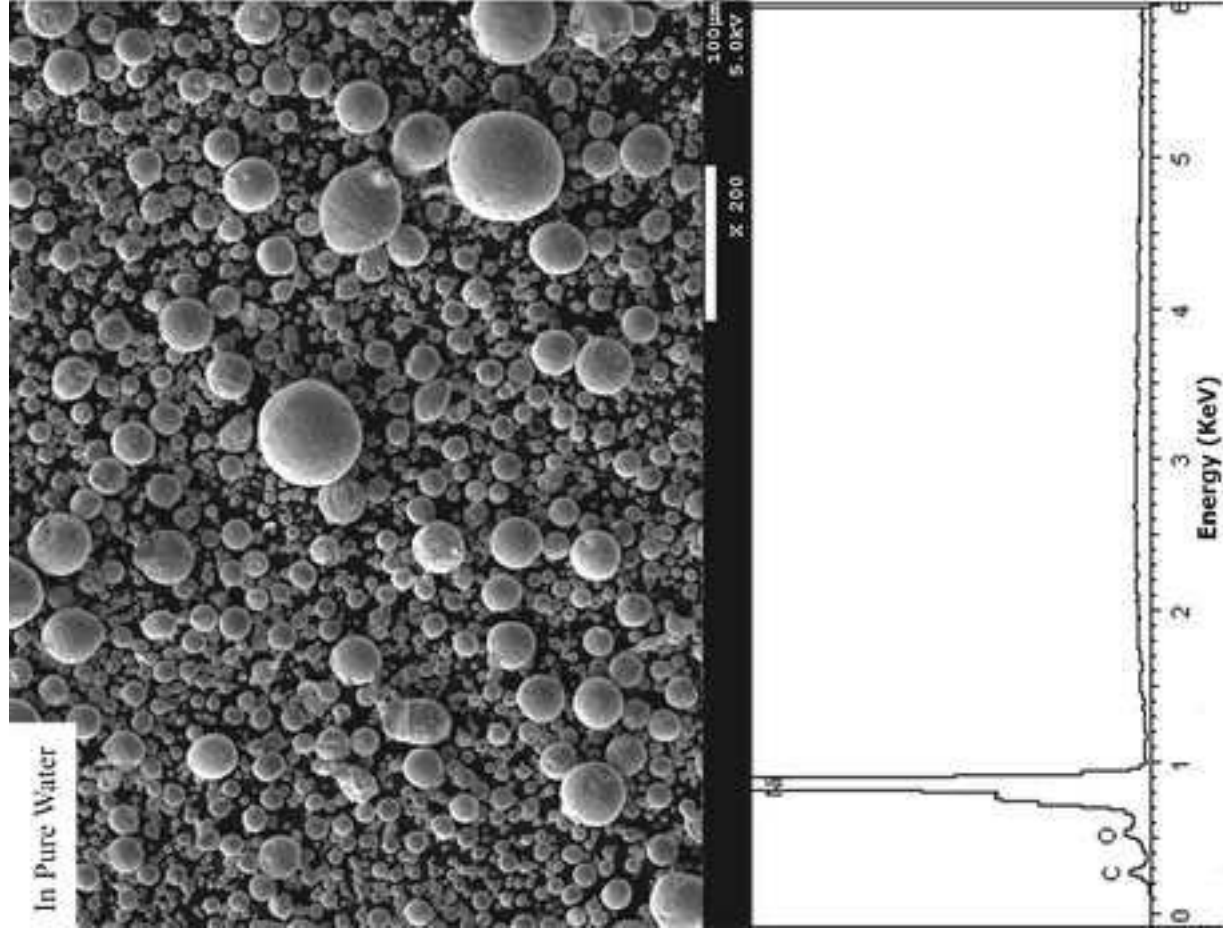


Figure 4
[Click here to download high resolution image](#)

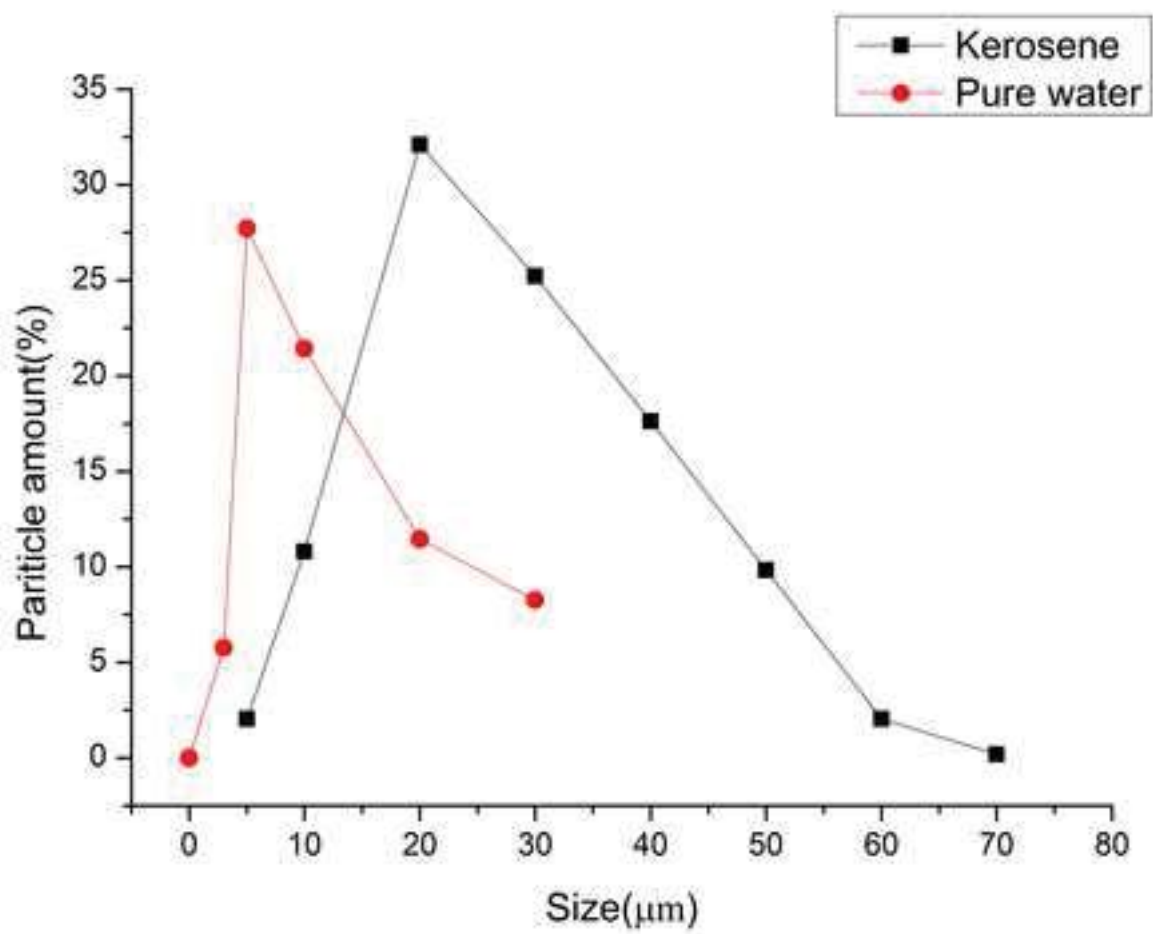
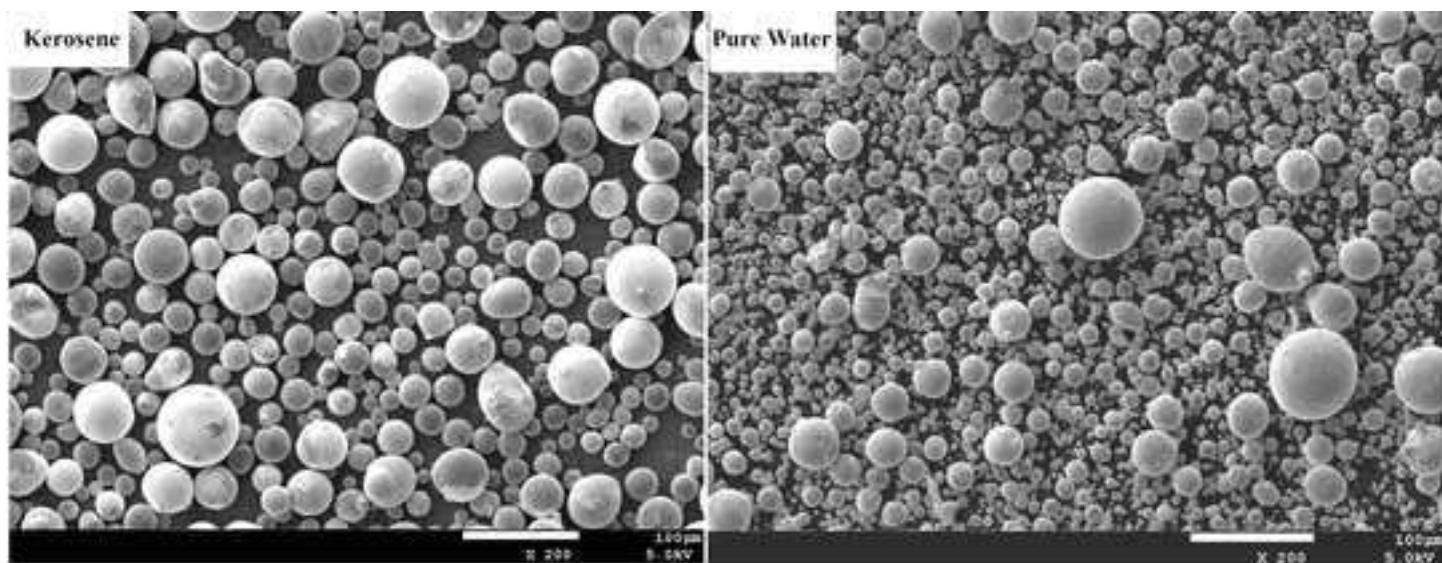


Figure 5
[Click here to download high resolution image](#)

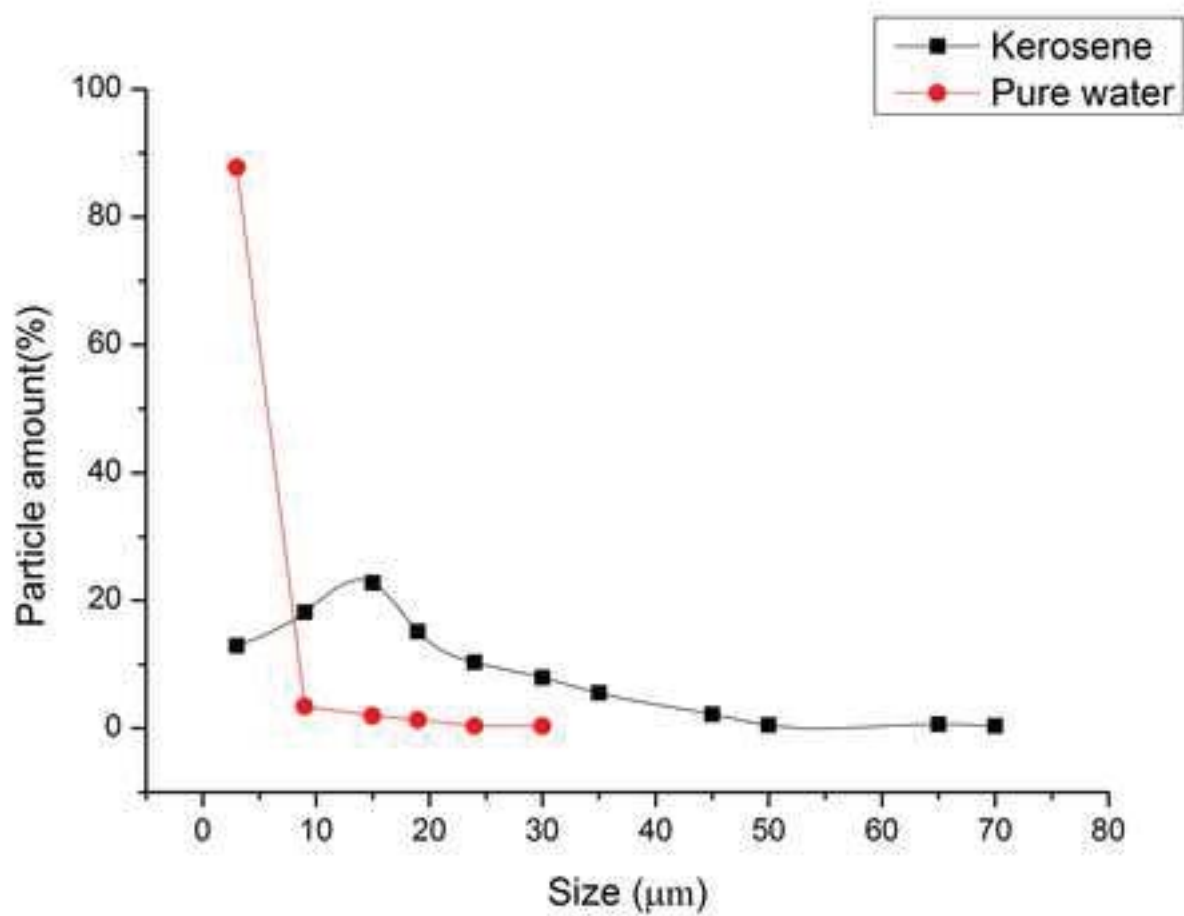
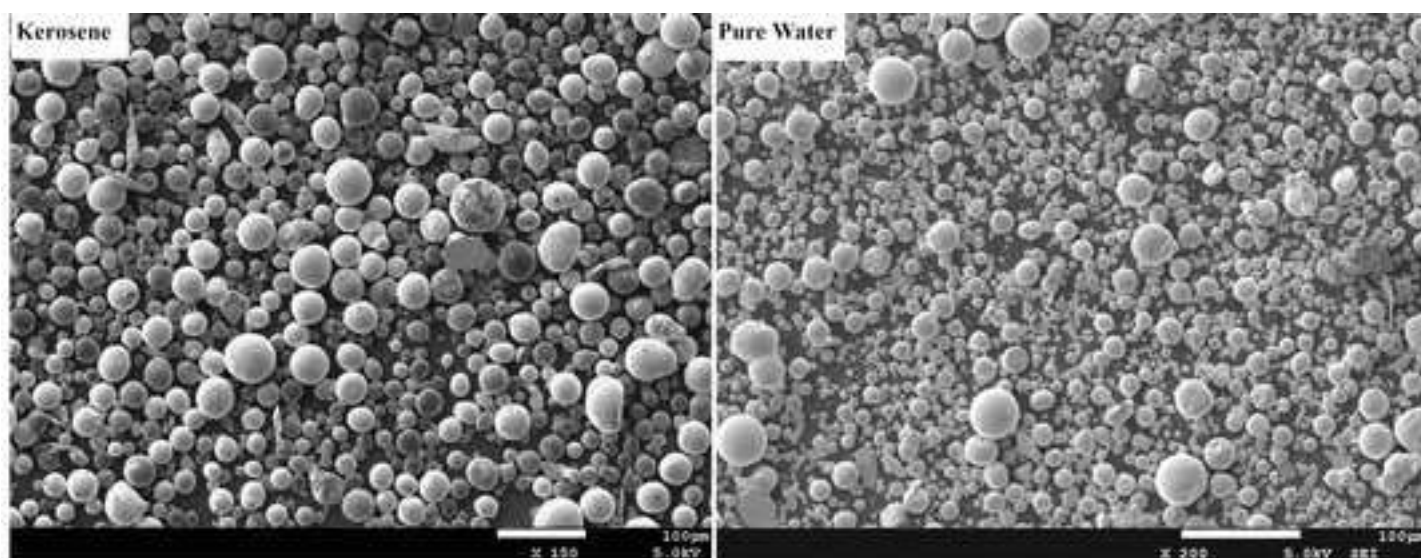
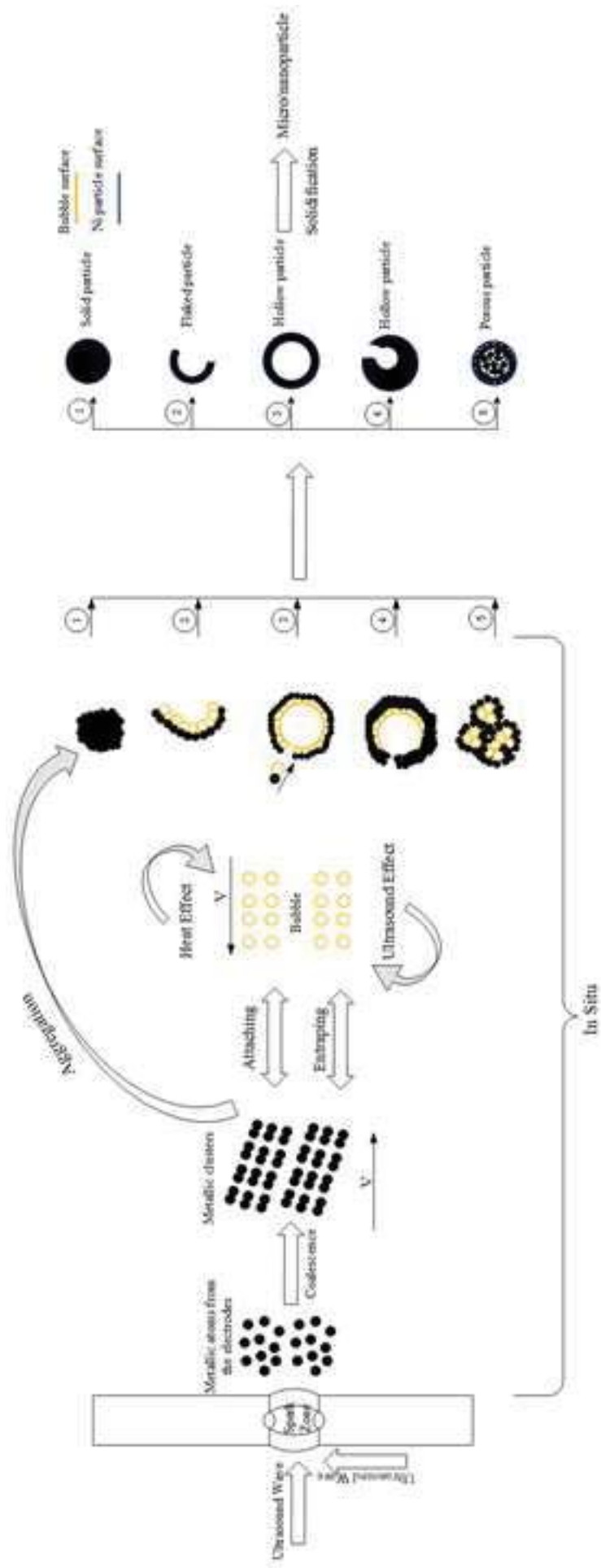


Figure 0
Click here to download high resolution image



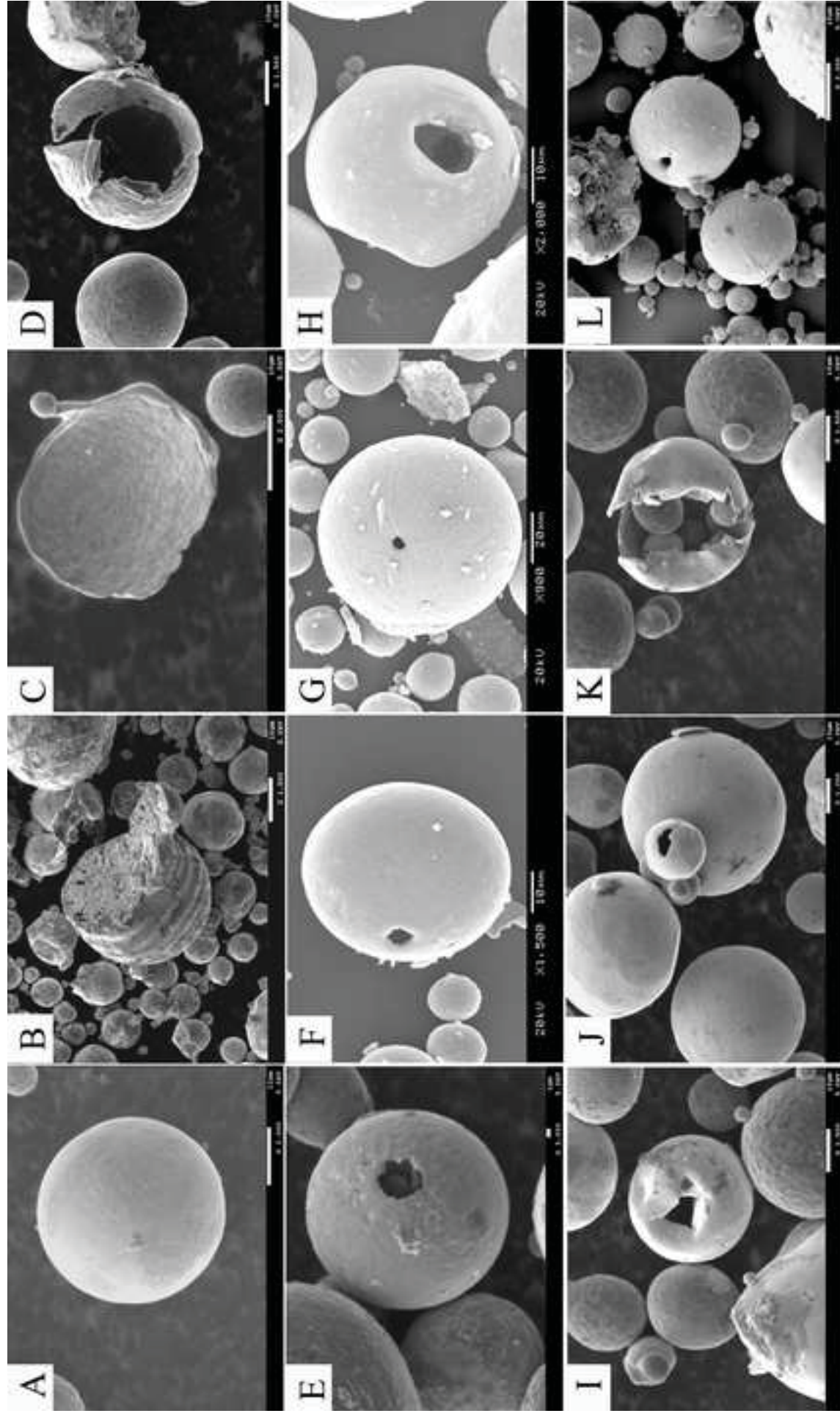


Table1. The physical characters of pure water and kerosene [29]

Dielectric Medium	Viscosity	Surface tension	Vapor pressure
	$10^{-6}(\text{m}^2/\text{s})$	$10^{-2}(\text{N/m})$	mmHg
Pure water	0.659	7.28	23.8
Kerosene	2.5-2.7	2.3-3.2	45-56

Table 2. The EDS analysis datasheet of Ni particles in different dielectric mediums

Elements	Mass (%)	
	Pure water	Kerosene
C	0.38	3.83
O	1.78	1.76
Ni	97.84	94.41
Totals	100	100

Figure Captions

Fig.1 The schematic illustration of experiment setup used for generating the Ni particles by ultrasound-aided Spark Discharge [28]

Fig.2 The SEM-EDS and XRD analysis of particles generated in the kerosene (Red bars correspond to JCPDS 65-0380.)

Fig.3 The SEM-EDS and XRD analysis of particles generated in the pure water (Red bars correspond to JCPDS 65-0380.)

Fig.4 Particle SEM features and size distribution comparison kerosene (black) and pure water (red) by Spark Discharge process

Fig.5 Particle size distribution comparison kerosene (black) and pure water (red) by ultrasound-aided Spark Discharge process

Fig.6 schematic illustration of procedures for generating metallic particles by ultrasound-aided spark discharge process

Fig.7 SEM micrograph of different structural particles generated by ultrasound-aided spark discharge process